Effect of Confinement on Proton Transfer Reactions in Water Nanopools

K.J. Tielrooij, M.J. Cox, and H.J. Bakker*
FOM Institute for Atomic and Molecular Physics [AMOLF]
Kruislaan 407 1098 SJ Amsterdam, The Netherlands

Proton transfer from the photoacid 8-hydroxy-1,3,6-pyrenetrisulfonic acid (HPTS) to water is studied in reverse micelles with ionic (AOT = sodium dioctyl sulfosuccinate) and non-ionic (BRIJ-30 = polyoxyethylene(4)lauryl ether) surfactants. The dynamics are studied by probing the transient electronic absorption and transient vibrational absorption, both with sub-picosecond resolution. The reverse micelle sizes range from approximately 1.6 to 5.5 nm in diameter. For both surfactants it is found that the rate of proton transfer decreases with decreasing reverse micelle size, regardless of surfactant. In addition, for AOT reverse micelles, a fraction of the photoacid molecules exhibit non-radiative decay, preventing proton transfer.

I. INTRODUCTION

Protons in water play an essential role in many chemical and biological processes. Photoacids are valuable for studying the transfer of protons to water because they are significantly more acidic in the excited electronic state than in the ground state. For these molecules the acidity can be switched by optical excitation, which makes it possible to start the proton transfer reaction at a well-defined point in time. A commonly used photoacid for these types of studies is 8-hydroxypyrene-1,3,6-trisulfonate (HPTS). The proton release from HPTS can be triggered by exciting HPTS with a 400 nm pulse. This excitation leads to an increase in acidity by a factor 10^6[1]. The subsequent proton transfer reaction ($ROH^* + H_2O \rightarrow RO^{-*} + H_3O^+$) can then be monitored with different optical techniques, including fluorescence emission and transient visible or mid-infrared absorption spectroscopy. In the visible region, the absorption and emission of electronically excited states of the acid (ROH^*) and the base (RO^{-*}) are used to probe the proton transfer reaction [2–14]. In the midinfrared region, the specific vibrational resonances of the photoacid, the photobase can also be monitored [15]. Additionally, a broad absorption band associated with the partially and fully hydrated proton makes it possible to monitor the uptake of the proton by the water solvent [16, 17].

In living organisms, water is commonly contained in very small volumes. As a result, protons are often dissolved in nanopools of water within a membrane [18]. The confinement of water and the interactions with the confining surfaces can have strong effects on the proton mobility. Similar effects can also arise in proton exchange membrane fuel cells, where a proton flows within a confined aqueous environment [19]. Reverse micelles are an exquisite model for studying confined water [20, 21]. Early studies of proton transfer in reverse micelles were done by Politi et al. [22, 23] and Bardez et al. [24, 25] using fluorescence measurements. It was observed that small reverse micelles have a decreased proton transfer rate, whereas larger reverse micelles exhibit the same dynamics as bulk water. More recently, the dynamics of protons in confined aqueous environments were studied in the optical regime using time-correlated single photon experiments with an instrument response function of 45 ps [26, 27]. These studies focused on confined water in Nafion fuel cell membranes. Additionally, reverse micelles were studied using AOT (sodium dioctyl sulfosuccinate) as the surfactant. The hydrophilic groups of AOT and Nafion are quite similar as they both contain sulfonate groups. For both systems the proton transfer was observed to slow down with decreasing water concentration [26, 27].

Here we investigate the dynamics of proton transfer from HPTS to water in confined aqueous environments using both electronic absorption in the visible range and vibrational absorption in the mid-infrared range, both with sub-picosecond time resolution. The water nanopools are formed by reverse micelles produced using two different types surfactants, ionic (AOT) and non-ionic one (BRIJ-30 = polyoxyethylene(4)lauryl ether). As a result, we can distinguish the effects of the confinement of the water from the effects of the specific interactions of the system with the surfactant.

II. EXPERIMENTAL

We performed pump-probe experiments in which we excite HPTS to an electronically excited state and probe either the transient electronic absorption of the photoacid and the conjugate photobase, or the transient vibrational response of the photoacid, the photobase and the hydrated proton. The 400 nm pump, the visible continuum probe, and the tunable infrared pulses are generated using non-linear frequency conversion of light from a commercial Ti:Sapphire regenerative amplified laser system (Spectra-Physics Hurricane). This system

*Electronic address: bakker@amolf.nl

produces 100 fs, 1 mJ pulses centered at 800 nm with a repetition rate of 1 kHz. The pump pulse centered at 400 nm come from frequency doubling of the 800 nm pulses with a β-Ba_2O_4 (BBO) crystal (2 mm, $\theta = 29°$). The pump beam is attenuated to about 1 μJ. The polarization of the pump beam is set at the magic angle (54.7 °) with respect to the probe polarization so that only isotropic signals are probed.

To generate the visible continuum probe pulses, we focus about 2 μJ of the 800 nm fundamental into a 3 mm thick z-cut sapphire substrate to generate a broadband continuum of wavelengths ranging from over 1000 nm to just below 400 nm. For probing the transient spectra of the photoacid and photobase we generally only use the wavelength range between 400 and 700 nm. The probe pulses are spectrally dispersed with a grating-based spectrograph (Roper Scientific) and detected with a home-built diode-array detector.

To generate the tunable mid-infrared probe pulses for the transient vibrational absorption experiments, a white-light seeded optical parametric amplifier (Spectraphysics OPA) converts the 800 nm fundamental into two tunable output pulses, signal (1200 - 1600 nm) and idler (1600 - 2400 nm). These pulses are separated and focused into a $AgGaS_2$ crystal (2 mm, $\theta = 45°$). Difference-frequency mixing the signal and idler pulses produces probe pulses that are tunable between 2.7 and 8 μm (3700 - 1250 cm^{-1}).

A computer controlled translation stage sets the relative delay between the pump and probe pulses and an optical chopper blocks every other pump pulse for active background subtraction. The probe pulse is split into two parts, one of which is focussed into the sample in spatial overlap with the pump pulse. The other is used as a reference to compensate for pulse-to-pulse intensity fluctuations. The sample is placed between CaF_2 windows that are separated by a teflon spacer of typically 100 - 200 μm thickness. The sample is rotated to avoid photo-product formation and long-term heating effects. The transmitted probe and reference pulses are spectrally dispersed with a spectrograph and detected with a 2×32 liquid-nitrogen cooled mercury-cadmium-telluride (MCT) array detector. We measure the pump-induced changes in absorption over a wide spectral range in the visible and mid-infrared as a function of delay time.

The reverse micelle samples are made by adding a solution of HPTS (8-hydroxy-1,3,6-pyrenetrisulfonic acid) in water to a mixture of surfactant and apolar solvent. We use two combinations of surfactant and solvent: AOT (sodium dioctyl sulfosuccinate) and isooctane, and BRIJ-30 (polyoxyethylene(4)lauryl ether) and cyclohexane. In both cases the molar ratio of surfactant and apolar solvent is 1:20. The concentration of HPTS in water is chosen such that each reverse micelle will contain a maximum of one HPTS molecule. The ratio between the concentration of water and the concentration of surfactant ($w = M_{H_2O}/M_{surf.}$) determines the size of the reverse micelles. For AOT reverse micelles we studied samples with w = 2, 3, 6, 8, 10 and 15; for BRIJ reverse micelles with w = 1, 2, 3, 4, 6, 8, 10, 15. These values of w correspond to diameters ranging from $\sim$ 1.6 nm to 5.5 nm [28] [29] [30] [31], where it should be noted that AOT reverse micelles have been characterized in greater detail. A reverse micelle with a diameter of 1.6 nm contains approximately 50 water molecules [30].

III. FIGURES

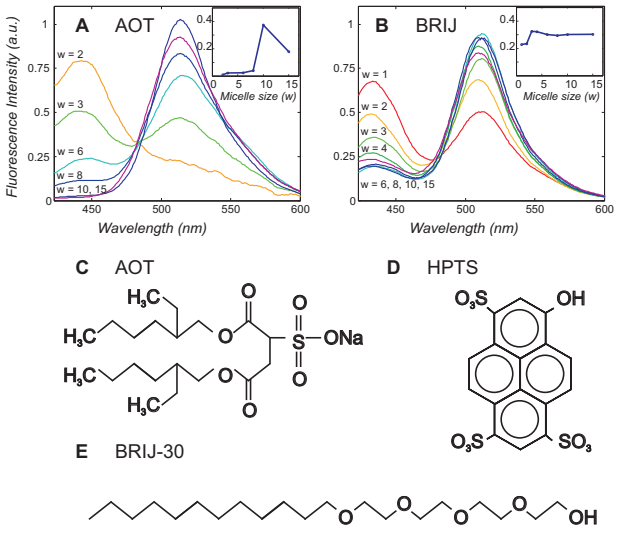

FIG. 1: Steady-state fluorescence spectra of HPTS in reverse micelles with AOT **(A)** as the surfactant and with BRIJ **(B)** as the surfactant. The insets show the fluorescence intensity integrated over the entire spectrum for different reverse micelle sizes. **C** The structural formula of AOT (sodium dioctyl sulfosuccinate). **D** The structural formula of HPTS (8-hydroxy-1,3,6-pyrenetrisulfonic acid). **E** The structural formula of BRIJ-30 (polyoxyethylene(4)lauryl ether).

IV. RESULTS

A. Steady-state Fluorescence

Figure 1 shows the fluorescence spectra of HPTS for AOT reverse micelle with w = 2 to 15 and BRIJ reverse micelle with w = 1 to 15. Here, the fluorescence spectrum of each sample is normalized to the total frequency-integrated fluorescence of that sample. The fluorescence peak at 440 nm corresponds to the excited photoacid ROH^*, and the peak at 520 nm corresponds

to the excited conjugate photobase RO^{-*}. For both AOT and BRIJ reverse micelles, the intensity of ROH^* increases relative to that of RO^{-*} with decreasing reverse micelle size. This finding agrees with previous observations, and shows that the proton uptake by water is reduced/slowed down in small reverse micelles [22, 24, 26]. For the AOT reverse micelles, the intensity of ROH^* completely vanishes for the larger reverse micelle sizes, showing that upon approaching the bulk limit practically all photoacid molecules release their proton well within the fluorescence lifetime. However, for the large BRIJ reverse micelles, there remains a small contribution centered at 520 nm. This could be caused by hydrogen bonding of the photoacid molecule to the surfactant, thereby preventing proton transfer.

The insets of figure 1 show the frequency-integrated fluorescence intensity as a function of reverse micelle size. These intensities are corrected for the different concentrations of HPTS in each individual sample. This correction is performed by measuring the absorption spectrum of each sample with a steady state UV-Visible spectrometer (Jasco V530) to determine the concentration. For the AOT reverse micelles, the integrated fluorescence becomes relatively small for $w < 10$. This observation indicates the presence of a quenching process in which the excited photoacid molecule undergoes non-radiative decay to the ground state ($ROH^* \rightarrow ROH$). For the BRIJ reverse micelles, the integrated fluorescence intensity does not show such a strong dependence on reverse micelle size. Only for very small reverse micelle sizes ($w \leq 2$), a slight decrease in the integrated fluorescence intensity is observed.

B. Femtosecond visible pump-probe

Figure 2 shows the transient visible absorption spectra at different delay times obtained for two different AOT reverse micelle sizes ($w = 15$ and $w = 8$). These spectra were collected using the visible pump-probe setup described in the experimental section. For large reverse micelles ($w = 15$), the transient spectra strongly resemble the transient spectra observed for a solution of HPTS in bulk water [14]. The spectra show an isosbestic point around 480 nm, indicating that the dynamics are dominated by an interconversion between two different distinct states (ROH^* and RO^{-*}). At early delay times, the spectrum shows a broad absorption centered near 500 nm that is due to the excited state absorption of the photoacid, ROH^*. At large delay times, the spectrum shows an absorption band at 440 nm that is due to the absorption of the excited state of the conjugate photobase RO^{-*}. The spectrum also shows a decrease in absorption at 510 nm due to stimulated emission of the photobase. This stimulated emission is also present at early delay times, but is overwhelmed by the absorption

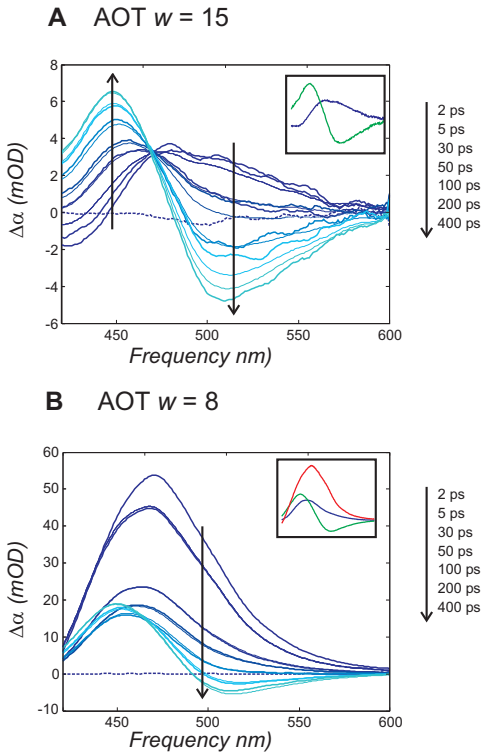

FIG. 2: Femtosecond visible absorption spectrum for AOT reverse micelles with $w = 15$ **(A)** and $w = 8$ **(B)**. Thick lines show the measured data; thin lines the fitted spectra using the model described in the text. The dotted arrows indicate the direction of pump-probe delay time. Insets show the decomposed spectra found by the model.

of the excited state of ROH^*. For medium size reverse micelles ($w = 8$), the spectra look very different and no longer show an isosbestic point as seen in figure 2B.

Figure 3 shows the time evolution of the transient absorption signals measured at wavelengths of 440 nm and 520 nm as a function of delay time. For large reverse micelles (figure 3A), the signals show a complementary rise and decay, reflecting the conversion of ROH^* to RO^{-*}. For medium size reverse micelles (figure 3B), both signals show an initial fast decay, followed by a slow rise at 440 nm (RO^{-*}) and a slow decay at 520 nm (ROH^{-*}).

Figure 4 shows the transient visible absorption at different delay times for two BRIJ reverse micelles ($w = 15$ and $w = 2$). For all BRIJ reverse micelles, the spectra are quite similar to the spectra observed for bulk water and for large AOT reverse micelles. The dynamics, however, do change with reverse micelle size, as is illustrated in figure 5. For large BRIJ reverse micelles (Fig. 5A), the dynamics are similar to bulk water and large AOT reverse micelles, showing a rise at 440 nm (RO^{-*}) and a complementary decay at 520 nm (ROH^*). For small BRIJ reverse micelles (Fig. 5B), there is a small-amplitude fast initial component, followed by a slow rise at 440 nm and a slow decay at 520 nm. The rise and decay are clearly

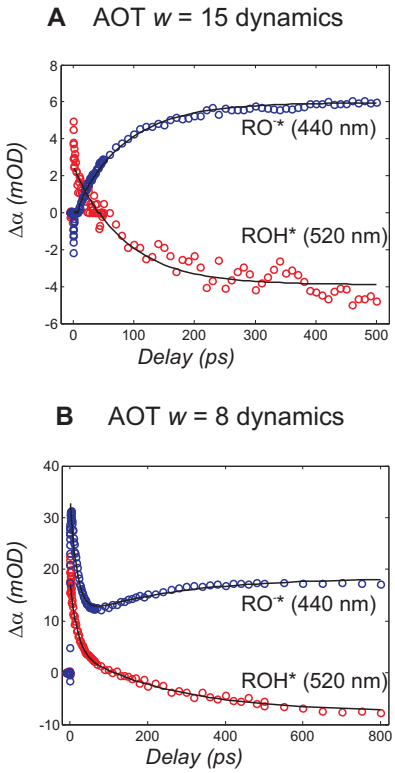

FIG. 3: **(A)** The signal as a function of pump-probe delay time at a wavelength of 440 and 520 nm for large reverse micelles ($w = 15$). The lines are obtained by fitting the data to eq. 1. **(B)** The signal as a function of pump-probe delay time at a wavelength of 440 and 520 nm for medium size reverse micelles ($w = 8$). The lines are obtained by fitting the data to eq. 2.

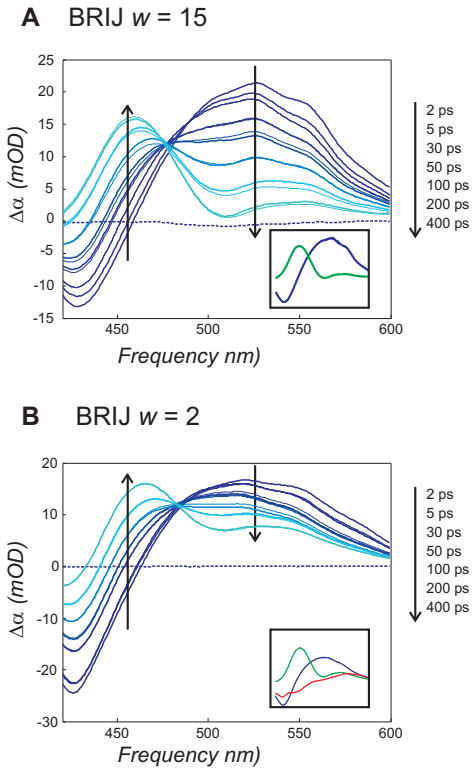

FIG. 4: Femtosecond visible absorption spectrum for BRIJ reverse micelles with $w = 15$ **(A)** and $w = 2$ **(B)**. Thick lines show the measured data; thin lines the fitted spectra using the model described in the text.

much slower than in the case of the large reverse micelles.

C. Femtosecond midinfrared pump-probe

Figure 6 shows the transient absorption spectra in the mid-infrared for two different AOT reverse micelles ($w = 15$ and $w = 6$) for varying delay times. These spectra were taken with the visible-mid-infrared pump-probe setup described in the experimental section. After excitation there is a direct rise of absorption bands at 1480 and 1540 cm^{-1}, which have been assigned to ROH^*. Due to the deprotonation, these bands decay and a new band grows in at 1503 cm^{-1}, representing the absorption of RO^{-*} [15] [16]. These vibrational bands likely represent combinations of aromatic ring distortional modes and stretching modes [32].

For large AOT reverse micelles ($w = 15$), the spectra in the 1500 cm^{-1} region are nearly identical to the corresponding spectra in bulk H_2O [16]. This finding agrees with the observations of the visible pump-probe data. For smaller reverse micelles ($w = 6$), the measured spectra differ strongly (figure 6B). These spectra do not show a rise of the deprotonated RO^{-*} band at 1503 cm^{-1}. In addition, the band of ROH^* at 1480 cm^{-1} is no longer observed.

Figure 7A shows the absorption of the photoacid vibration at 1545 cm^{-1} as a function of delay time for four different AOT reverse micelle sizes. The transient signals show the presence of an initial fast component for which the amplitude increases with decreasing reverse micelle size. We also probe the transient spectra in the frequency range between 1850 and 1950 cm^{-1}, which contains the broadband infrared absorption that is attributed to the partially/fully hydrated proton [16] [17]. Figure 7B shows the signal of the partially/fully hydrated proton as a function of delay time for four different reverse micelle sizes. Again, for large reverse micelles ($w = 15$), the dynamics are similar to that observed for bulk liquid water [16]. As the reverse micelle size decreases, the dynamics develop a fast initial component, similar to what is observed for the dynamics of the ROH^* band at 1540 cm^{-1}.

In figure 8, transient mid-infrared absorption spectra measured at different delays are shown for BRIJ reverse micelles with $w = 15$ and $w = 2$. A striking difference with the mid-infrared spectra observed for the AOT reverse micelles (Fig. 6), is that for BRIJ reverse micelles

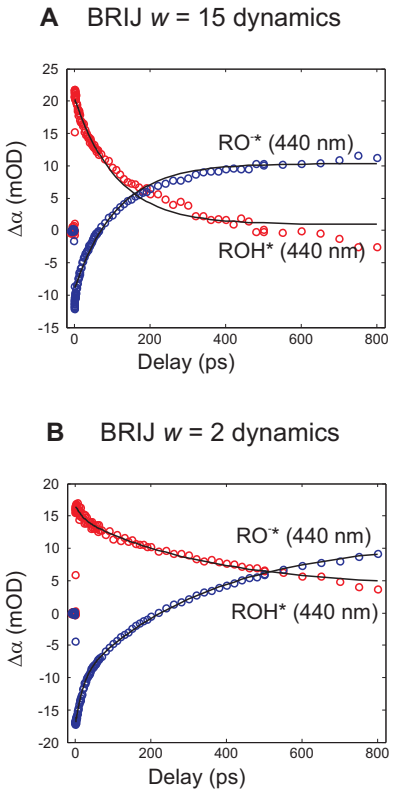

FIG. 5: Delay scans at two frequencies with corresponding fits for $w = 15$ **(A)** and $w = 2$ **(B)**.

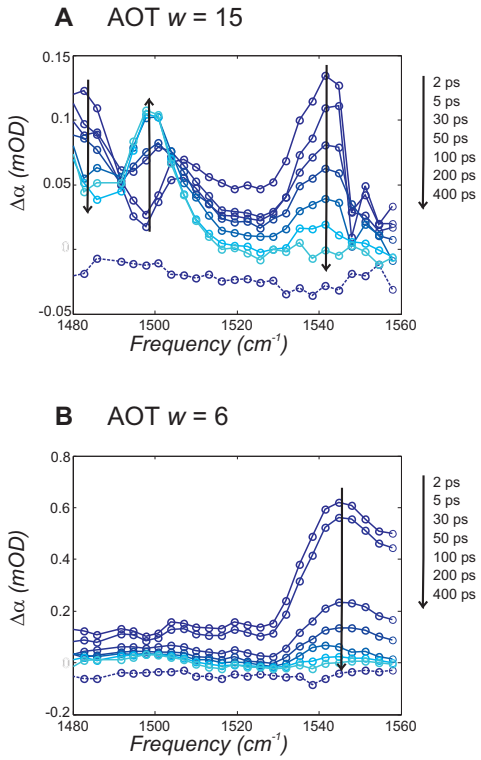

FIG. 6: Femtosecond midinfrared absorption spectrum showing decaying acid bands (ROH*) at 1480 and 1545 cm^{-1} and a rising base band (RO^{-*}) at 1500 cm^{-1} for an AOT reverse micelle $w = 15$ **(A)**. For a smaller reverse micelles with $w = 6$ only the decay of the acid band at 1545 cm^{-1} is observed **(B)**.

the spectra do not change much with reverse micelle size. Only the RO^{-*} band at 1500 cm^{-1} shows a somewhat less pronounced rise for $w = 2$, indicating that there is less deprotonation in this smaller reverse micelle.

V. DISCUSSION

For HPTS dissolved in large AOT and BRIJ reverse micelles ($w \geq 10$), the shapes and dynamics of the transient electronic and vibrational spectra are very similar to what is observed for HPTS dissolved in bulk liquid water. This finding is consistent with earlier results from fluorescence measurements and time-correlated photon counting [22, 24, 26] on proton transfer in reverse micelles. It also corresponds well with the observation that water in large reverse micelles shows very similar molecular dynamics as in bulk water [33–36].

To analyze our results in more detail, we use the excited state proton transfer scheme in figure 9. For large reverse micelles, we model the transient visible spectra with two spectral components and one interconversion time constant. This time constant is used as a global fit parameter that is fixed for all wavelengths. Hence, we fit the following equation to the absorption change $\Delta\alpha(\omega, t)$:

$$\Delta\alpha(\omega, t) = A_2(\omega) + \left[A_1(\omega) - A_2(\omega)\right] \cdot e^{-k_{PT}t}, \qquad (1)$$

with A_1 and A_2 the spectra of the two components and k_{PT} the interconversion rate. The spectra $A_1(\omega)$ and $A_2(\omega)$ represent the absorption spectra of ROH^* and RO^{-*}, respectively, and k_{PT} represents the rate at which the proton is released from ROH^*. We start the fit after 5 ps, after the fast initial dynamics - the Stokes shift ($\sim$ 1 ps) and contact-ion pair formation ($\sim$ 3 ps) - are complete. The contact ion-pair formation corresponds to a charge transfer state with a weakened OH bond of the photoacid, but for which proton dissociation has not yet taken place [14] [37]. The spectra obtained from the fit to Eq. 1 for the AOT and BRIJ reverse micelles are shown in the insets of figures 2 and 4, respectively. The fits to the dynamics are shown with the solid lines in figures 3 and 5.

For large AOT and BRIJ reverse micelles ($w = 15$), we find $k_{PT} = (84\pm5 \text{ ps})^{-1}$ and $(110\pm5 \text{ ps})^{-1}$, respectively. These values agree well with the bulk value for the proton transfer rate of $(90 \text{ ps})^{-1}$ [5, 14]. Similar dynamics are observed for the vibrational bands of the photoacid and the photobase. For $w = 15$ AOT and BRIJ reverse

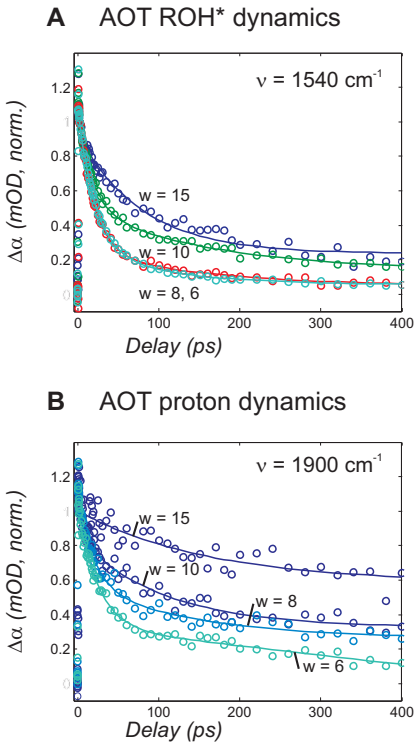

FIG. 7: **A** The dynamics of the ROH^* band around 1540 cm^{-1} for a range of reverse micelle sizes ($w = 15, 10, 8$ and 6). **B** The dynamics of the proton continuum averaged between 1850 and 1950 cm^{-1} for the same range of reverse micelle size.

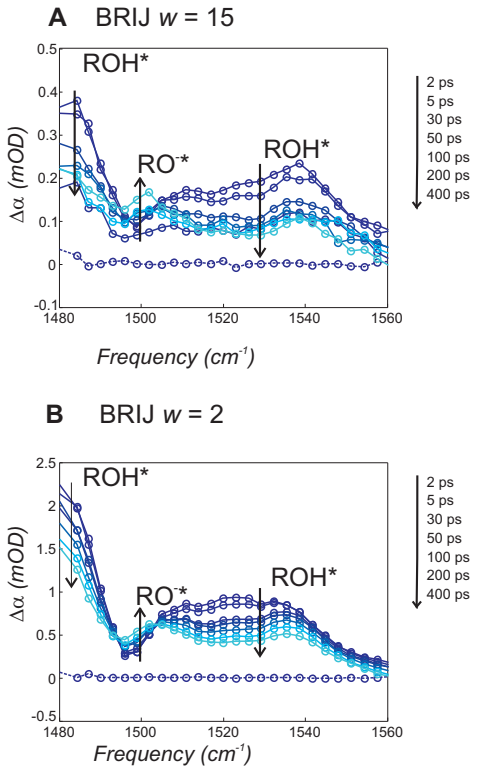

FIG. 8: Femtosecond midinfrared absorption spectrum with decaying acid bands (ROH^*) around 1480 and 1545 cm^{-1} and rising base band (RO^{-*}) around 1500 cm^{-1} for BRIJ reverse micelles with $w = 15$ **(A)** and $w = 2$ **(B)**.

micelles, the dynamics of the vibrational ROH^* band at 1540 cm^{-1} can be fit well with a single-exponential function. For the AOT reverse micelle we find a rate constant of $(89\pm10$ ps$)^{-1}$, and for the BRIJ reverse micelle a value of $(129\pm15$ ps$)^{-1}$.

For smaller reverse micelles with $w < 8$, the dynamics of the transient electronic and vibrational spectra strongly differ from what is observed for bulk liquid water and large reverse micelles. Especially in the case of AOT reverse micelles, we see a number of changes occurring between w = 10 and w = 8. We observe this both in the steady-state fluorescence data and the time-resolved differential absorption measurements. First of all, the electronic absorption spectrum is vastly different for $w = 8$ (figure 2). The signal corresponding to ROH^* (at 520 nm) contains a large component that disappears on a fast timescale (figure 3). Furthermore, the vibrational spectrum is very different for $w = 6$ (figure 6) and also includes a similar fast component (figure 7A). Finally, the proton continuum for small AOT reverse micelles shows a strong initial decay with a similar time constant (7B). So clearly, the time-resolved measurements indicate that during this fast initial process ROH^* disappears, without RO^{-*} or a proton signal (H_3O^+) being formed. From the scheme in figure 9 it is clear that this process corresponds to non-radiative decay of ROH^* to its ground state ROH.

For small AOT reverse micelles, this effect is much more pronounced than for the BRIJ reverse micelles. For both reverse micelle systems, the amplitude of the fast contribution increases with decreasing reverse micelle size. This finding and the observation that the fluorescence intensity becomes smaller for decreasing reverse micelle sizes (figure 1), indicate that the fast initial component comes from a rapid non-radiative decay. Therefore, we model the transient absorption measurements for smaller reverse micelles with two parallel processes: the conversion of ROH^* to RO^{-*} (deprotonation) and the quenching of ROH^* to ROH. We also include the possibility that the spectrum of the HPTS molecules that undergo a rapid non-radiative decay differs from the spectrum of the HPTS molecules that undergo deprotonation. For small reverse micelle sizes ($w \leq 8$) we use the following equation to fit the observed absorption changes:

$$\begin{aligned}\Delta\alpha(\omega,t) &= A_2(\omega) + \left[A_1(\omega) - A_2(\omega)\right] \cdot e^{-k_{PT}t} \\ &\quad + A_3(\omega) \cdot e^{-k_q t}\end{aligned} \quad (2)$$

$A_3(\omega)$ corresponds to the electronic absorption spectrum of HPTS molecules that undergo quenching with rate constant k_q. For all small reverse micelle sizes with

$w < 8$ we obtain a good fit of the transient electronic using equation (2). In addition, we find that the spectra A_1 and A_2 are nearly identical to the corresponding spectra for large reverse micelles ($w \geq 10$). Additionally, for both AOT and BRIJ reverse micelles ($w < 8$), we find a quenching rate constant (k_q) of about 20 ps^{-1}, regardless of the reverse micelle size. As expected, the amplitude of the contribution from the spectrum A_3 increases for smaller reverse micelles. As the amount of quenching depends on the nature of the surfactant and increases with decreasing reverse micelle size, it seems likely that the quenching results from HPTS molecules that are hydrogen-bonded to the surfactant.

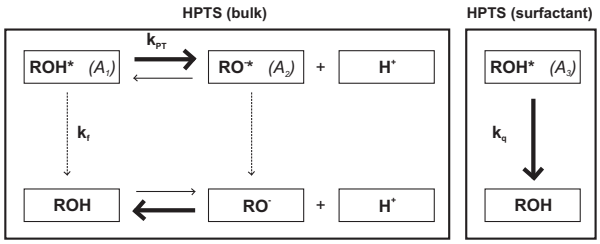

FIG. 9: Scheme describing the dynamics of HPTS, with k_{PT} the proton transfer rate, k_f the fluorescence rate and k_q the quenching rate. In brackets we show the electronic absorption spectra from equations 1 and 2 that correspond to that state.

The two parallel processes likely correspond to two distinct species of HPTS molecules: HPTS (bulk), which exhibits proton transfer, and HPTS (surfactant), which gets quenched (see the scheme in figure 9). For AOT reverse micelles, HPTS (surfactant) presumably binds to one of the negatively charged sulfonate groups. This hydrogen bond will result in a change in the electronic structure of the HPTS molecule resulting in a different transient absorption spectrum ($A_3(\omega)$ versus $A_1(\omega)$). The change in electronic structure will also influence the vibrational spectrum, especially the absorption bands of the aromatic ring modes. Indeed it is found that the ROH^* band at 1480 cm^{-1} shows a strong decrease in relative amplitude compared to the ROH^* band at 1540 cm^{-1} with decreasing reverse micelle size. The band at 1480 cm^{-1} has been assigned to a combination band of stretch and aromatic ring deformation modes [32], and is expected to be affected by the change in the electronic structure configuration of the HPTS molecule.

The transient vibrational absorption measurements show very similar dynamics to the transient electronic absorption measurements. Therefore we use a similar fitting scheme for the vibrational absorption measurements. For larger reverse micelles, ($w \geq 10$, the measured transient absorption signals are fit to a single exponential decay (Eq. 1). Similarly, for smaller reverse micelles ($w \leq 8$), the transient vibrational absorption signals measured for AOT reverse micelles are fit to a bi-exponential decay (Eq. 3), one exponent representing the quenching process, the other exponent the proton transfer. The fast process has a time constant of 20 ps^{-1}, in good agreement with the transient electronic absorption measurements.

For medium size AOT reverse micelles ($w = 8$), the proton transfer rate k_{PT} is observed to slow down to (221 ps)$^{-1}$. This observation is in good quantitative agreement with previous measurements of HPTS in AOT reverse micelles [22, 24, 26] and 2-naphtol-6,8-disulfonate in AOT reverse micelles [13]. For the smallest AOT reverse micelles ($w = 2$, $w = 3$ and $w = 6$), the signal is strongly dominated by the quenching contribution, making it impossible for us to extract a reliable deprotonation rate. However, HPTS in BRIJ reverse micelles shows minimal quenching, and we can deduce the time constant of the proton transfer, even for the small BRIJ reverse micelle ($w = 2$). For this reverse micelle size we find a time constant of proton transfer of 350 ps, which indicates that the proton transfer is slowed down by a factor of 4 in comparison to bulk liquid water.

For AOT and BRIJ reverse micelles we observe a slowing down of the proton transfer process with decreasing reverse micelle size. This slowing down appears to be caused by the confinement of the water volume, and not by specific interactions with the surfactant, as the HPTS molecules that do interact with the surfactant show rapid quenching. The slowing down of the proton transfer with decreasing reverse micelle size can be explained by the fact that the rate of proton transfer to water is largely determined by the orientational motion of water molecules [38–40]. The reorientation of the water molecules is slowed down considerably in reverse micelles [33–35], particularly in the region near the surfactant layer.

VI. CONCLUSIONS

We studied the effect of the confinement of water on the rate of proton transfer using femtosecond visible and mid-infrared pump-probe spectroscopy. As model systems we study reverse micelles of different sizes and of different surfactant composition. We study reverse micelles with an anionic surfactant (AOT) and with a non-ionic surfactant (BRIJ-30). For both types of reverse micelles, we observe that for large reverse micelles ($w = 15$) the proton transfer shows a similar rate constant (k_{PT}=($\sim$90 ps)$^{-1}$) as is observed in bulk liquid water.

For small reverse micelles ($w \leq 8$), we observe two distinct decay processes. Some of the excited photoacid molecules are observed to become rapidly quenched after excitation, with a rate k_q of ($\sim$20 ps)$^{-1}$. This fraction is much larger for AOT reverse micelles than

for BRIJ reverse micelles, and the relative quenching contribution increases with decreasing reverse micelle size. The quenching is likely caused by specific interactions between HPTS and the surfactant molecules. The remaining fraction of the excited photoacid molecules undergo proton transfer with a slower rate than in bulk liquid water. For small BRIJ reverse micelles with $w = 2$, we observe a time constant for proton transfer of 350 ps, which is about 4 times slower than in bulk liquid water. The decrease of the size of the nanopool leads to a similar slowing down of the proton transfer reaction for ionic and non-ionic surfactants. Therefore, this slowing down appears not to be caused by specific interactions with the surfactant, but rather by the confinement of the water volume.

[1] A. Weller, *Progress in Reaction Kinetics Vol. 1*, Pergamon Press New York, **1961**.

[2] M.J. Politi and J.H. Fendler, *J. Am. Chem. Soc.* **1984**, *106*, 265-273.

[3] E. Pines and D. Huppert, *Chem. Phys. Lett.* **1986**, *126*, 88-91.

[4] E. Pines and D. Huppert, *J. Chem. Phys.* **1986**, *84*, 3576-3577.

[5] E. Pines, D. Huppert, and N. Agmon, *J. Chem. Phys.* **1988**, *88*, 5620-5630.

[6] N. Agmon, E. Pines, and D. Huppert, *J. Chem. Phys.* **1988**, *88*, 5631-5638.

[7] E. Pines, D. Huppert and N. Agmon, *J. Phys. Chem.* **1991**, *95*, 666-674.

[8] H. Agmon, D. Huppert, A. Masad and E. Pines, *J. Phys. Chem.* **1991**, *95*, 10407-10413.

[9] K. M. Solntsev, D. Huppert, N. Agmon, and L. M. Tolbert, *J. Phys. Chem. A* **2000**, *104*, 4658-4669.

[10] T.-H. Tran-Thi, T. Gustavsson, C. Prayer, S. Pommeret, and J. T. Hynes, *Chem. Phys. Lett.* **2000**, *329*, 421-430.

[11] J. T. Hynes, T.-H. Tran-Thi, and G. Granucci, *J. Photochem. Photobiol. A* **2002**, *154*, 3-11.

[12] P. Leiderman, L. Genosar, and D. Huppert, *J. Phys. Chem. A* **2005**, *109*, 5965-5977.

[13] B. Cohen, D. Huppert, K. M. Solntsev, Y. Tsfadia, E. Nachliel, M. Gutman, *J. Am. Chem. Soc.* **2002**, *124*, 7539-7547.

[14] D.B. Spry, A. Goun and M.D. Fayer,*J. Phys. Chem. A* **2007**, *111*, 230-237.

[15] M. Rini, B.Z. Magnes, E. Pines, and E. T. J. Nibbering, *Science* **2003** , *301*, 349-352.

[16] B.J. Siwick and H.J. Bakker, *J. Am. Chem. Soc.* **2007**, *129*, 13412-13420.

[17] M.J. Cox and H.J. Bakker, *J. Chem. Phys.* **2008**, *128*, 174501 1-10.

[18] N. Nandi, K. Bhattacharyya and B. Bagchi, *Chem. Rev.* **2000**, *100*, 2013-2045.

[19] T.A. Zawodzinski, M. Neeman, L.O. Sillerud, S. Gottesfeld, *J. Phys. Chem.* **1991**, *95*, 6040-6044.

[20] P. L. Luisi, B. E. Straub, Eds., Reverse Micelles: Biological and Technological Relevance of Amphiphilic Structures in Apolar Media, Plenum, New York, **1984**.

[21] N.E. Levinger, *Science* **2002**, *298*, 1722-1723.

[22] M.J. Politi, O. Brandt and J.H. Fendler, *J. Phys. Chem.* **1985**, *89*, 2345-2354.

[23] M.J. Politi and H.J. Chaimovich, *J. Phys. Chem.* **1986**, *90*, 282-287.

[24] E. Bardez, B. T. Goguillon, E. Keh, B. Valeur , *J. Phys. Chem.* **1984**, *88*, 1909-1913.

[25] E. Bardez, E. Monnier and B. Valeur, *J. Phys. Chem.* **1985**, *89*, 5031-5036.

[26] D. B. Spry, A. Goun, K. Glusac, D. E. Moilanen, and M. D. Fayer, *J. Am. Chem. Soc.* **2007**, **111**, 8122-8130.

[27] D. E. Moilanen, D. B. Spry, M. D. Fayer, *Langmuir* **2008**, *24*, 3690-3698.

[28] M. Zulauf and H.-F. Eicke, *J. Phys. Chem.* **1979**, *83*, 480-486.

[29] T. Kinugasa, A. Kondo, S. Nishimura, Y. Miyauchi, Y. Nishii, K. Watanabe, and H. Takeuchi, *Colloids and Surfaces A* **2002**, *204*, 193-199.

[30] M. Vasilescu and A. Caragheorgheopol, *Langmuir* **1995**, *11*, 2893-2898.

[31] D. Pant and N.E. Levinger, *Langmuir* **2000**, *16*, 10123-10130.

[32] O. Mohammed, D. Pines, J. Dreyer, E. Pines, and E. T. J. Nibbering, *ChemPhysChem* **2005**, *6*, 625-636.

[33] I. Piletic, D. E. Moilanen, D. B. Spry, N. E. Levinger, M. D. Fayer,*J. Phys. Chem. A* **2006**, *110*, 4985-4999.

[34] D.E. Moilanen, N. E. Levinger, D. B. Spry, and M. D. Fayer, *J. Am. Chem. Soc.* **2007**, *129*, 14311-14318.

[35] A.M. Dokter, S. Woutersen and H.J. Bakker, *Proc. Nat. Ac. Sci. USA* **2006**, *103*, 15355-15358.

[36] D. S. Venables, K. Huang and C.A. Schmuttenmaer,*J. Phys. Chem. B* **2001**, *105*, 9132-9138

[37] D.B. Spry and M.D. Fayer, *J. Chem. Phys.* **2008**, *128*, 084508 1-9.

[38] J.D. Bernal and R.H. Fowler, *J. Chem. Phys.* **1933**, *1*, 515-548.

[39] M. Tuckerman, K. Laasonen, M. Sprik, M. Parrinello, *J. Phys. Chem.* **1995**, *99*, 5749-5752.

[40] N. Agmon, *Chem. Phys. Lett.* **1995**, *244*, 456-462.

[41] This work is part of the research program of the "Stichting voor Fundamenteel Onderzoek der Materie (FOM)", which is financially supported by the "Nederlandse organisatie voor Wetenschappelijk Onderzoek (NWO)".